Inviscid Rotational Flows Near a Corner and Within a Triangle

Yong Kweon Suh*
School of Mechanical and Industrial System Engineering, Dong-A University

Solutions of inviscid rotational flows near the corners of an arbitrary angle and within a triangle of arbitrary shapes are presented. The corner-flow solution has a rotational component as a particular solution. The addition of irrotatoinal components yields a general solution, which is indeterminate unless the far-field condition is imposed. When the corner angle is less than 90° the flow asymptotically becomes rotational. For the corner angle larger than 90° it tends to become irrotational. The general solution for the corner flow is then applied to rotational flows within a triangle (Method I). The error level depends on the geometry, and a parameter space is presented by which we can estimate the error level of solutions. On the other hand, Method II employing three separate coordinate systems is developed. The error level given by Method II is moderate but less dependent on the geometry.

Key Words : Rotational Flow, Corner, Triangle, Poisson Equation

1. Introduction

Recently there has been an increased interest in the spin-up of fluids in non-axisymmetric containers such as rectangles (van Heijst, 1989; van Heijst, Davies and Davis, 1990; van Heijst, Maas and Williams, 1994; van de Konijnenberg, Wessels and van Heijst, 1996; van de Konijnenberg and van Heijst, 1996, 1997; Suh, 1994; Suh and van Heijst, 2000). In this case the starting flow, governed by a uniform vorticity (twice the angular speed of the container), separates from side walls immediately after rotation. The boundary-layer separation in turn causes gathering of vorticity near each corner, and the corner eddy is thus generated. The corner eddies play crucial a role in the subsequent flow dynamics and mixing within the container (van de Konijnenberg and van Heijst, 1996).

The fundamental question in this case would be: what is the basic mechanism of the corner-eddy generation and can we predict the eddies' growth rate? The present study has been motivated by the need of finding asymptotic solutions of a rotational flow field near a corner given at the very beginning of the spin-up process. In fact, the solution is a prerequisite for modelling of the corner-flow separation.

The corner-flow solution is then used as a basis in obtaining the rotational flow inside a triangular domain. The solution is important in itself. However, it also serves as an example that contains a corner and shows the asymptotic nature predicted by the corner-flow analysis. The solutions for the triangular domain are further validated by comparing them with those given by a second method.

A two-dimensional rotational flow driven by a uniform vorticity near a 90°-corner flow has already been considered by Moore, Saffman and Tanveer (1988). Their interests were in obtaining the steady separated flow using Batchelor's model. Although Batchelor's model itself is not of our concern, their solution to the 90°-corner region will be shown to be a special case of the present general solution valid for any arbitrary corner angle. Also, as far as the author knows, no results have been reported on the rotational flow field

* **E-mail** : yksuh@mail.donga.ac.kr
TEL : +82-51-200-7648; **FAX** : +82-51-200-7656
School of Mechanical and Industrial System Engineering, Dong-A University, Pusan 604-714.
(Manuscript **Received** December 22, 2000; **Revised** March 9, 2001)

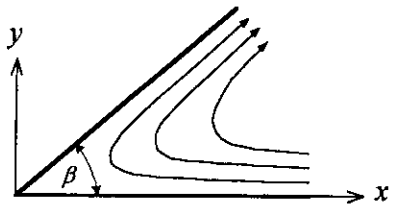

Fig. 1 Sketch of the corner flow and the Cartesian coordinates

near corners of arbitrary angles or inside triangles.

2. Corner Flows

2.1 Basic solution

We consider a Poisson equation

$$\nabla^2\psi=-2 \tag{1}$$

where ψ is a stream function, and ∇^2 denotes the two-dimensional Laplacian operator in the coordinates (x, y). Here, all of the variables are dimensionless, and the right-hand side of Eq. (1) represents the nondimensional counterpart of the uniform vorticity caused by an abrupt rotation alout the axis normal to the plane under consideration. The minus sign in (1) stems from the fact that in most rotating flow experiments the table's rotations are counterclockwise so that the vorticity inducing the relative motion is positive.

As stated in the introduction, our first interest is a corner of arbitrary angle β as shown in Fig. 1. Impermeable restrictions are used as boundary conditions on the lower and upper walls;

$$\psi=0 \text{ on } y=0 \text{ and } y=mx, \tag{2}$$

where $m=\tan\beta$ is the slope of the upper boundary.

The particular solution to Eqs. (1) and (2) are $\psi_p=-y(y-mx)$, or in terms of the polar coordinates (r, θ),

$$\psi_p=-\frac{1}{2}r^2(1-\cos2\theta)-\frac{1}{2}mr^2\sin2\theta \tag{3}$$

2.2 An example of general solution

Although the solution above satisfies both Eqs. (1) and (2), we can consider adding to Eq. (3) an infinite number of complementary solutions ψ_h satisfying the Laplace equation $\nabla^2\psi_h=0$ and the impermeable conditions in Eg. (2). One example with no singularity in the field is a class of functions

$$\psi_h=r^{kn}\sin kn\theta$$

for an arbitrary integer $k\geq1$. Here, $n=\pi/\beta$. As a special case, we choose the smallest number, $k=1$. Then a complete solution takes the form

$$\psi=-\frac{1}{2}r^2(1-\cos2\theta)-\frac{1}{2}mr^2\sin2\theta+Cr^n\sin n\theta \tag{4}$$

where C is an arbitrary constant. (We will see shortly that with this choice the solution for the critical case, $\beta=\pi/2$, can be effectively obtained.)

The addition of the complementary solution can give rise to a cellular flow pattern near the corner. The size of the cell may be represented by r_0(i.e. the value of r at $\theta=0$) at which $\partial\psi/r\partial\theta$, the radial velocity component, vanishes; thus, the point at $r=r_0$ may be called the detachment point. Taking the derivative of Eq. (4) with respect to θ, evaluating at $\theta=0$ and setting the result zero gives the relation between r_0 and C as follows.

$$C=\frac{m}{n}r_0^{2-n} \tag{5}$$

Substituting this back into Eq. (4) then yields the corner-flow solution having a detachment point on the lower wall at $r=r_0$.

In the following, we consider two special cases, at which m becomes infinite ($n=2$) or the cell tends to an equilateral triangle ($n=3$).

At $n=2$, m becomes infinite, and the second and third terms in Eq. (4) also tend to infinity. However it can be shown that in the limit $n\to2$, the two terms after being summed can be reduced to a regular function. In this case Eq. (4) takes the following form.

$$\psi=-\frac{1}{2}r^2\left[1-\cos2\theta+\frac{2}{\pi}\{(2\ln r/r_0-1)\sin2\theta+2\theta\cos2\theta\}\right] \tag{6}$$

This corresponds to the solution given by Moore et al. (1988). If the complementary solution Cr^n

$n\theta$ were not included in Eq. (4), no regular solution can be obtained for the critical case $n=2$.

For $n=3$, the slope m is $\sqrt{3}$, and Eq. (4) becomes simply

$$\psi=-y(y-\sqrt{3}x)(1-x-y/\sqrt{3}) \tag{7}$$

Here $r_0=1$ is assumed without the loss of generality. Thus ψ is also zero on the straight line $x+y/\sqrt{3}=1$. This means that the solution Eq. (7) corresponds to the starting flow within an equilateral triangle of unit side length. The solution was also given by Milne-Thomson (1968).

We also note that $m=0$ for $n=1$, and the solution in this case simply becomes a shear flow, $\psi=-y^2$.

We are further interested in r_c, the value of r at the centerline $\theta=\beta/2$, at which $\psi=0$. This corresponds to the radial distance along the centerline from the corner to the boundary of the cell. It can be shown that

$$r_c=r_0\left(\frac{n}{2}\tan\frac{\pi}{2n}\right)^{1/(n-2)} \tag{8}$$

for $n\neq 2$ and

$$r_c=r_0\exp\{(2-\pi)/4\}$$

for $n=2$. In fact r_c decreases monotonously with β from $r_c=r_0$ at $\beta=0$ to $r_c=0$ at $\beta=\pi$, the latter corresponding to an infinitely thin cell.

Figure 2 shows typical solutions for four corner angles. We can see that for (a) and (b) ($n<3$), the detaching streamline is convex and for (d) ($n>3$), it is concave relative to the corner. As analysed previously, at the critical value $n=3$, (c), the detaching streamline becomes straight.

2.3 Asymptotic Nature of the Corner Flow

The general solution Eq. (4) is of a special kind, and we can consider adding $r^{kn}\sin kn\theta$ with $k>1$. In fact the importance of each mode is related to the flow condition in the region far from the corner. A good example is the flow within a triangle which will be analysed in the following section. However, for a concave corner (i.e. for $n>1$), the asymptotic nature of flows in the region $r\to 0$ is not affected by the terms with $k>1$.

More importantly, the asymptotic nature is fundamentally different depending on whether n is larger or smaller than 2. For $n<2$, the dominant term in Eq. (4) is $Cr^n\sin n\theta$. Thus, the

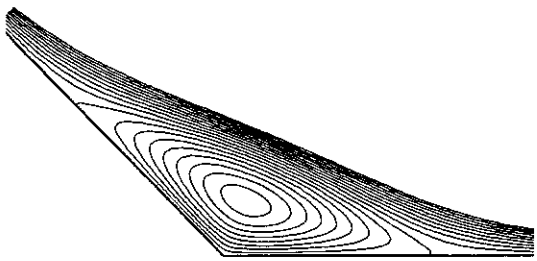

(a) $n=4/3$

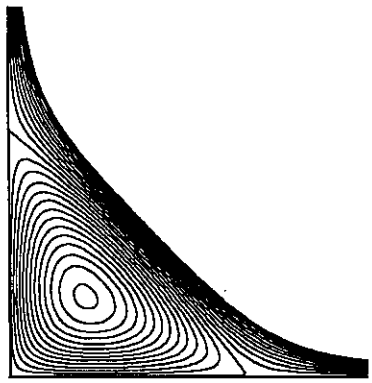

(b) $n=2$

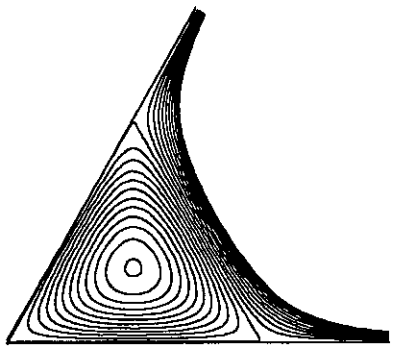

(c) $n=3$

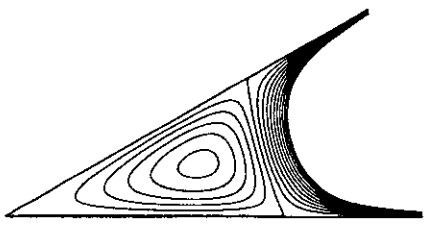

(d) $n=6$

Fig. 2 Streamlines in corners for four n values. $\Delta\psi=0.005$

asymptotic corner-flow is governed primarily by the far-flow condition. This means that the corner flow is asymptotically of the irrotational type. On the other hand, for $n>2$, the dominant terms of Eq. (4) are of $O(r^2)$, and thus it is not affected by the far-flow condition. Thus, the corner flow is asymptotically of the rotational character. Such observations are important for modelling the starting rotational flow in containers having corners.

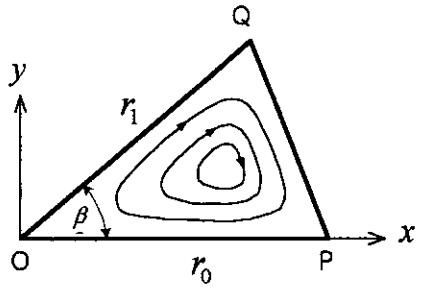

Fig. 3 Sketch of the rotational flow within a triangle and the Cartesian coordinates

3. Flows Within a Triangle

3.1 Method I

Using ϕ_p the particular solution for the corner, i.e. Eq. (3), as a basis, we can write the solution of Eq. (1) for a triangular domain as

$$\phi=\phi_p+\sum_{k=1}^{K} C_k r^{kn}\sin kn\theta \tag{9}$$

where C_k denotes arbitrary constants to be determined such that the impermeable condition on the third boundary

$$\phi=0 \text{ on } r=r_t(\theta) \tag{10}$$

is satisfied. The function $r_t(\theta)$ defined as

$$r_t(\theta)=\frac{r_0 r_1\sin\beta}{r_0\sin\theta+r_1\sin(\beta-\theta)} \tag{11}$$

represents the straight line constituting the third boundary PQ, and r_1 is the length of the boundary OQ (Fig. 3).

For Eq. (9) to satisfy Eq. (10) in a least square sense, we multiply both sides of Eq. (9) by $r^{jn}\sin jn\theta$, apply $r=r_t(\theta)$, and integrate over the range $0\le\theta\le\beta$ to obtain the following linear system of equations.

$$A_{jk}C_k=B_j \ (j,\ k=1,\ 2,\ \cdots,\ K) \tag{12}$$

where

$$A_{jk}=\int_0^\beta r_t^{(k+j)n}\sin kn\theta\sin jn\theta d\theta$$

$$B_j=-\int_0^\beta \phi_p(r_t,\ \theta)r_t^{jn}\sin jn\theta d\theta$$

The system of equation in Eq. (12) is solved by using the LU-decomposition method.

3.2 Method II

A second method for solving Eq. (1) under the boundary conditions Eqs. (2) and (10) has been developed. It uses three separate coordinate systems (x_1, y_1), (x_2, y_2), and (x_3, y_3) with origins at the corresponding apex O, P and Q, respectively, and aligned as shown in Fig. 4. The ith side having length l_i lies on the x_i-axis, and the distance from the side to the apex not lying on the side is denoted as d_i.

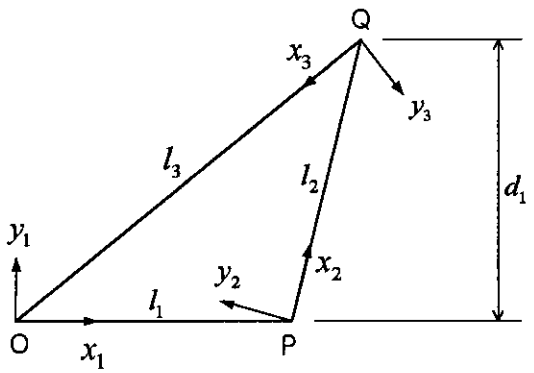

Fig. 4 Three separate coordinate systems for Method II

Then the solution ϕ can be written as

$$\phi=\phi_0+\sum_{i=1}^{3}\phi_i, \tag{13}$$

where

$$\phi_0=y_1(y_1-d_1)$$

$$\phi_i=\sum_{k=1}^{Ki} a_{ik}\sinh\{k\pi(d_i-y_i)/l_i\}\sin(k\pi x_i/l_i)$$

Note that ϕ_0 is a particular solution written in terms of (x_1, y_1), and ϕ_1 the complementary solution written in terms of (x_i, y_i). Also Eq. (13) gives $\phi=0$ at three apex.

To obtain a_{ik}, we require $\phi=0$ on each boundary and use the Fourier expansion method. For in-

stance, on side 2, the corresponding equation is

$$\sum_{k=1}^{K1} a_{2k}\sinh(k\pi d_2/l_2)\sin(k\pi x_2/l_2) = -\psi_0(x_2, 0) - \sum_{i=1,3}\psi_i(x_i(x_2, 0), y_i(x_2, 0)) \quad (14)$$

This again reduces to a linear system similar to Eq. (12) for the unknowns a_{2k} when both sides are multiplied by $\sin p\pi x_2/l_2$, where p is an integer, and integrated over $0 \leq x_2 \leq l_2$. The unknowns a_{1k} and a_{3k} contained implicitly in the righthand side of Eq. (14) are assumed to be known, and an iteration method is used to obtain the converged values of a_{ik}. To evaluate the righthand side of Eq. (14), we must know the relationship between (x_2, y_2) and (x_i, y_i). This relation can be established in two steps: $(x_2, y_2) \rightarrow (X, Y) \rightarrow (x_i, y_i)$, where (X, Y) are the global coordinates, which may be the same as (x_1, y_1), and the equation of transformation in each step can be obtained easily.

3.3 Numerical results

Figure 5 shows typical results given by Method I with $K=10$ for three shapes. The second case (b) in principle can be obtained directly by using Eq. (4), but here it is calculated from Eq. (3) with β very close to $\pi/2$.

The first two solutions are reasonable. These patterns are invariant if K is increased to 20 or decreased to 5. However, case (c) shows wiggles near the third boundary (line PQ) on which the Fourier expansion method is applied to obtain a_{ik}. The pattern does not improve even if K is increased significantly. The reason for this irregular pattern is not clear, but it commonly occurs when the difference between corner angles at P and Q is quite large. However, a smooth, reasonable solution to this case can be obtained when the side OP is taken as the third boundary instead of PQ. The resulting pattern is the same as that in (a). In fact, the parameters for (c) are chosen so that the triangle is congruent with (a).

The wiggles shown in Fig. 5(c) are directly related to the fact that the boundary condition on the third boundary is not satisfied. Thus, as a quantity measuring such wiggles, it is natural to

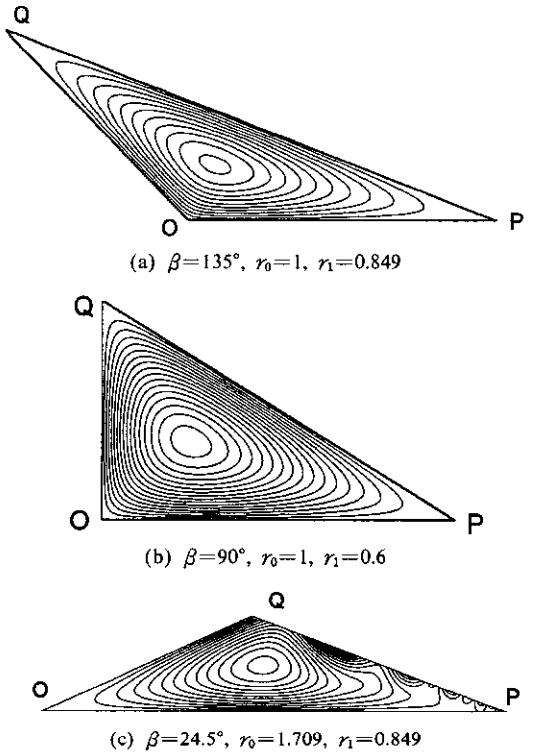

(a) $\beta=135°$, $r_0=1$, $r_1=0.849$

(b) $\beta=90°$, $r_0=1$, $r_1=0.6$

(c) $\beta=24.5°$, $r_0=1.709$, $r_1=0.849$

Fig. 5 Streamlines obtained by Method I for three cases. $\Delta\psi=0.002$

introduce ψ_ε defined as

$$\psi_\varepsilon = \frac{1}{Al_t}\oint |\psi| dl \quad (15)$$

where l denotes the coordinate along the whole path of the three sides and l_t the total length. The quantity is referenced to area A because the representative value of ψ(e.g. the maximum value of $|\psi|$) is of $O(A)$. Of course the exact proportionality holds only when the triangles are similar.

Figure 6 shows the distribution of ψ_ε in the parameter space (x_Q, y_Q), the coordinates of the apex Q, calculated for $r_0=1$. As mentioned above, the errors are greater in the region where the two corner angles on both edges of the third boundary are larger, e.g. $y_Q<0.2$, $0.1<x_Q<0.7$. Therefore, to obtain a reasonable solution by Method I, care must be given to selecting a proper choice of (x_Q, y_Q), as implied in Fig. 5(c). For instance the geometry of Fig. 5(c) after being scaled by a facton of 1.709 gives $(x_Q, y_Q)=(0.452,$

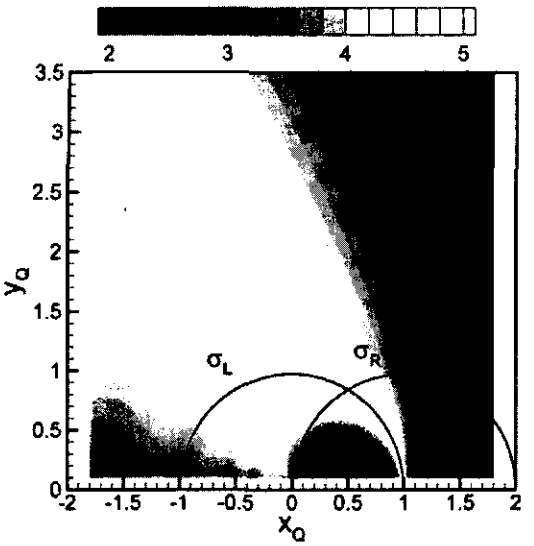

Fig. 6 Distribution of ϕ_ϵ in the parameter space (x_Q, y_Q) obtained by Method I; $r_0=1$. The level number indicates $-\log_{10}\phi_\epsilon$

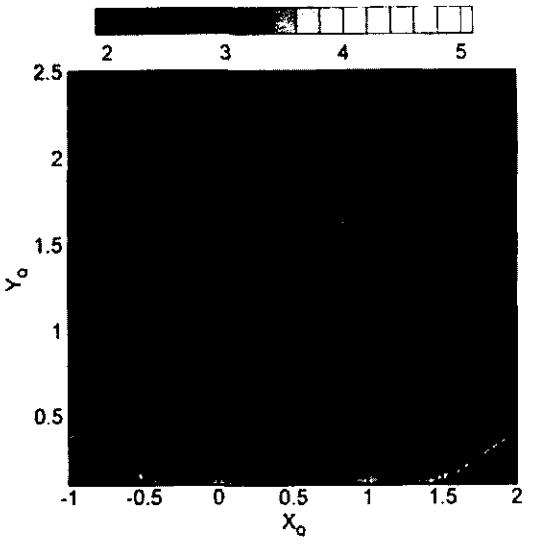

Fig. 8 Distribution of ϕ_ϵ in the parameter space (X_Q, Y_Q) obtained by Method II. $l_1=1$. The level number indicates $-\log_{10}\phi_\epsilon$

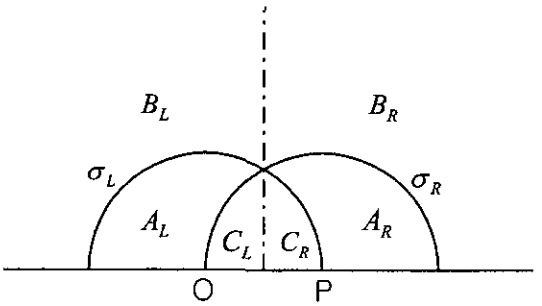

Fig. 7 Six subregions associated with the similarity relations between triangles

0.205). This parameter set is indeed in the region of relatively high error (Fig. 6). We can find two triangles similar to this one, while the third apex Q spans the space, the apex O and P being fixed at (0, 0) and (0, 1) respectively. The first similar triangle has its apex Q′ on the extended line PQ with PQ′==1/PQ, and is called the inverse mapping based on P (hereinafter referred to as I_R). The second one has its apex Q′ on the extension of OQ with OQ′=1/OQ, which is called the inverse mapping based on O (hereinafter referred to as I_L); The two are symmetric with respect to the line $x=1/2$(called the horizontal mapping; H). The first one corresponds to Fig. 5 (a), and this gives a reasonable solution. However the latter results in relatively high error as can be checked from Fig. 6.

Using the above notations, and referring to Fig. 7 we now show that the finite region A_L can produce all the possible shapes of triangles. As can be seen from Fig. 7, all regions other than A_L can be mapped to A_L as follows.

$$A_R \xrightarrow{H} A_L$$

$$B_R \xrightarrow{H} B_L \xrightarrow{I_L} A_L$$

$$C_R \xrightarrow{H} C_L \xrightarrow{I_R} A_L$$

The region A_L is selected as the reference because it gives the least error as can be seen in Fig. 6 However, the region close to the circle σ_R and the origin has larger errors than the horizontally symmetric one near the circle σ_R(Fig. 6).

Compared with Method I, Method II provides more evenly distributed ϕ_ϵ as shown in Fig. 8. However, the overall error level is rather high, and the regions of slow convergence or no convergence (black region in the figure) exist.

Figure 9 shows level plots of ϕ obtained by Method II for the three cases in Fig. 5. We note

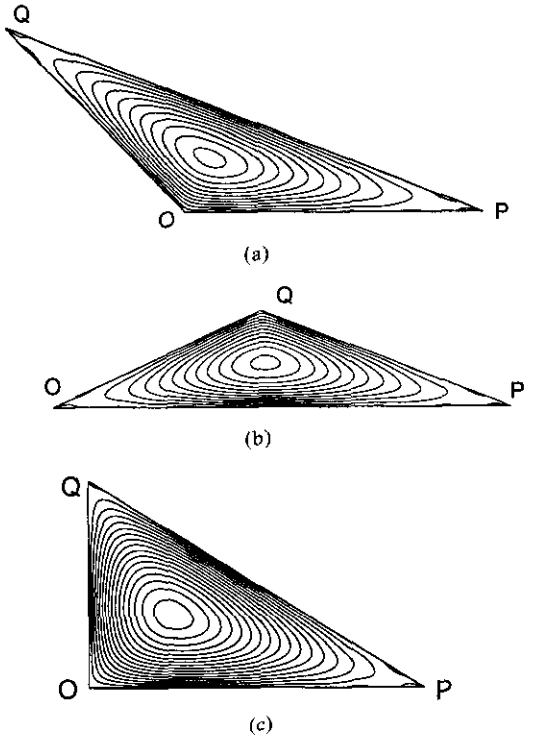

Fig. 9 Streamlines obtained by Method II for the three triangles of Fig. 5(a), (b), and (c). $\Delta\psi=0.002$

slight wiggles near the corners in all cases. However, (c) looks remarkably smoother than Fig. 5(c).

Conclusively, Method II gives solutions of moderate errors, and the error level is uniform over the space (X_0, Y_0). However more accurate solutions can be obtained by using Method I.

4. Conclusive Remarks

Inviscid rotational flow near a corner can be described by a simple analytic solution. The solution reveals two types of asymptotic behavior depending on the corner angle β. For $\beta>90°$, the far-flow condition prevails the asymptotic flow in the corner, and for $\beta<90°$, it is independent of the far-flow condition.

The flow within a triangle was described by the corner-flow solution containing both rotational and irrotational componerts. Aside from the importance in itself, the solution serves as an example of using the corner-flow solution in analysing the asymptotic flow structure near the corners of polygonal domains.

Since two methods employing different coordinate systems exhibit basically identical solutions, we can infer that both solution methods presented in this paper are reliable.

Acknowledgement

This research has been supported from the Basic Research Program of the Korea Science and Engineering Foundation, grant No. 2000-1-30400-002-3

References

van Heijst, G.J. F., 1989, "Spin-up Phenomena in Non-Axisymmetric Containers," *J. Fluid Mech.*, Vol. 206, pp. 171~191.

van Heijst, G.J. F., Davies, P.A. and Davis, R. G., 1990, "Spin-up in a Rectangular Container," *Phys. Fluids*, Vol. A2, pp. 150~159.

van Heijst, G.J. F., Maas, L.R. M. and Williams, C. W. M., 1994, "The Spin-up of Fluid in a Rectangular Container with a Sloping Bottom," *J. Fluid Mech.*, Vol. 265, pp. 125~159.

Henderson, D.M., Lopez, J.M. and Stewart, D. L., 1996, "Vortex Evolution in Non-Axisymmetric Impulsive Spin-up from Rest," *J. Fluid Mech.*, Vol. 324, pp. 109~134.

van de Konijnenberg, J.A., Wessels, T.L. and van Heijst, G.J. F., 1996, "Spin-up in a Circular Tank with a Radial Barrier," *Phys. Fluids*, Vol. 8, pp. 2048~2059.

van de Konijnenberg, J.A. and van Heijst, G.J. F., 1996, "Spin-up in a Rectangular Tank with a Discontinuous Topography," *Phys. Fluids*, Vol. 8, pp. 2943~2952.

van de Konijnenberg, J.A. and van Heijst, G.J. F., 1997, "Free-Surface Effects on Spin-up in a Rectangular Tank," *J. Fluid Mech.*, Vol. 334, pp. 189~210.

Milne-Thomson, L.M., 1968, *Theoretical Hydrodynamics*, Macmillan, London.

Moore, D.W., Saffman and Tanveer, S., 1988, "The Calculation of Some Batchelor Flows: The

Sadovskii Vortex and Rotational Corner Flow," *Phys. Fluids*, Vol. 31, pp. 978~990.

Suh, Y.K., 1994, "Numerical Study on Two-Dimensional Spin-up in a Rectangle," *Phys. Fluids*, Vol. 6, pp. 2333~2344.

Suh, Y.K. and van Heijst, G.J. F., 2000, "Spin-up in a Rectangular Container with an Internal Cylindrical Obstacle," *Phys. Fluids*, Vol. 12, pp. 1986~1996.